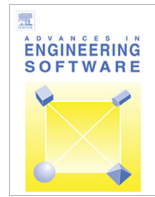




Contents lists available at SciVerse ScienceDirect

Advances in Engineering Softwarejournal homepage: www.elsevier.com/locate/advengsoft**Processing of fiber architecture data for finite element modeling of 3D woven composites****Andrew Drach, Borys Drach, Igor Tsukrov****Department of Mechanical Engineering, University of New Hampshire, 33 Academic Way, Durham, NH 03824, USA***ARTICLE INFO****Article history:**

Received 14 February 2013

Received in revised form 16 May 2013

Accepted 6 June 2013

Available online xxxx

Dedicated to Professor Zdeněk Bittnar in occasion of his 70th birthday.

Keywords:

3D woven composite

Meso-scale

Geometry repair

Finite element models

Effective elastic properties

As-woven reinforcement

ABSTRACT

An efficient procedure to process the textile simulation data and generate realistic finite element meshes of woven composites is proposed. The textile topology data in point cloud format is used to identify individual yarns, interpolate their cross-sectional contours, and generate smooth yarn surfaces. A robust algorithm to repair possible interpenetrations between yarn surfaces is developed and implemented in MATLAB. A 3D finite element mesh of the unit cell of composite material is generated based on the obtained yarn surfaces. The anisotropic material properties of the constituents are assigned with proper orientations.

The procedure is successfully applied to generate four finite element models with 1–10 million degrees of freedom. The models are used to predict effective elastic properties of an orthogonal 3D woven composite. The sensitivity of results to the level of finite element discretization is investigated.

© 2013 Elsevier Ltd. All rights reserved.

1. Introduction

Realistic simulations of 3D woven composites require accurate representation of the complex reinforcement structure of these materials. On the meso-scale, their structure can be described as a dual-phase system consisting of the bundles of fibers (*yarns* or *tows*) embedded in the matrix, as illustrated in Fig. 1. Depending on the direction of reinforcement, the yarns are identified as longitudinal (*warp*), transverse (*weft*) and through-thickness (*binder*). The configuration illustrated in Fig. 1 is the so-called 1x1 orthogonal architecture. This configuration is characterized by the binder yarns going vertically (up or down) through the entire thickness of composite at each crossing with the weft yarns column. At the micro-scale, yarns consist of several thousands of individual fibers, as illustrated in Fig. 1.

The goal of this paper is to develop an efficient procedure to construct finite element (FE) models on the meso-scale for various reinforcement architectures. Such models are usually developed based on the nominal geometry of composites. They are constructed from the weaving technological schematics (as in Fig. 2a) with a chosen shape of yarn cross-sections (Fig. 2b). This approach has been extensively discussed in the literature [1,2]

and implemented in such software packages as TexGen, WiseTex, DYNAFAB and ScotWeave. Note that another class of approaches based on the volumetric subdivisions known as “mosaic” models [3,4] is not considered in this paper.

The relative ease of nominal geometry model preparation introduces, however, some limitations to the approach. Modeling of architectures with a large volume fraction of reinforcements or a large number of binder yarns is difficult due to the inability of the approach to account for the deformations of yarn cross-sections during manufacturing. This leads to the geometric incompatibility problem which is manifested in the interpenetration of yarn cross-sections (Fig. 2c). Several authors [5–7] have developed remedial procedures including semi-automatic deformations of the yarn shapes, reductions of their cross-sectional area, and special procedures to prescribe changes in cross-sectional area and/or axial rotation of yarns. However, even for the geometries that can be modeled successfully, the artificially prescribed shape of cross-sections does not provide accurate description of the actual microstructure as observed in micrographs, see for example [8]. Actual geometry deviates from the nominal one due to the effect of tensile and contact pressure forces during the weaving process, and thermally induced stresses during the resin curing. These manufacturing processes lead to the deformation of nominal geometry at both micro- and meso-scales.

* Corresponding author. Tel.: +1 (603) 862 2086; fax: +1 (603) 862 1865.

E-mail address: igor.tsukrov@unh.edu (I. Tsukrov).

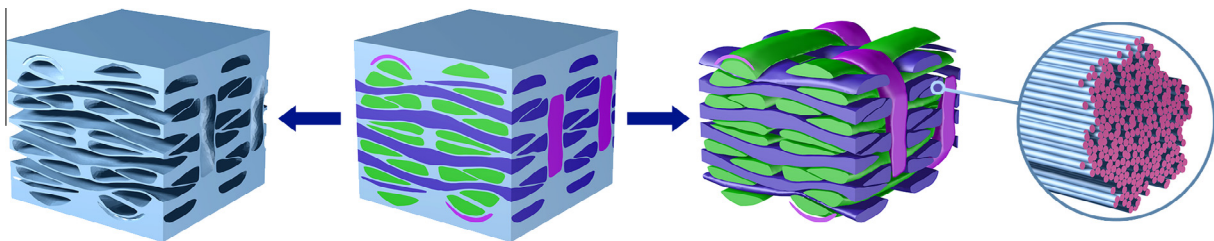


Fig. 1. Material structure of 3D woven composites on meso- and micro-scale.

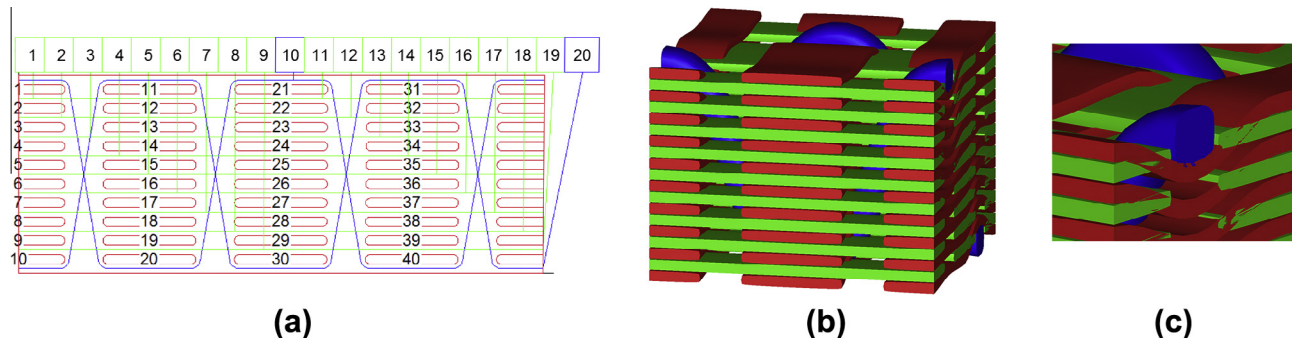


Fig. 2. Representation of 1×1 orthogonal reinforcement architecture as (a) technological schematics and (b) nominal solid yarn model. (c) Example of yarn interpenetration.

The limitations of “nominal geometry” approach can be addressed by utilizing a more realistic as-woven geometry of reinforcement. However, reproduction of as-woven geometry requires complicated textile mechanics simulations. An approach developed by Wang et al. [9–11] involves use of the so-called “multi-chain digital element analysis”. The yarns are represented as bundles of digital elements which are modeled as a series of interconnected rods (similar to FE truss elements). To obtain the as-woven geometry, deformation of the yarns is modeled as a step-by-step process of applying tension forces to the yarns, subdividing the yarns in more digital elements and relaxing the stresses. The contact between yarns is simulated by the special contact elements. This approach is implemented in DEA Fabric Mechanics Analyzer (DFMA) software (<http://www.fabricmechanics.com>) by the original authors of the method. The output of simulation results is organized as reinforcement surface mesh (STL format) or point cloud data.

In this paper, the authors propose an efficient procedure for development of meso-scale FE models for 3D woven composites based on the as-woven geometry presented as point cloud data. The proposed method provides a semi-automated flexible framework for conversion of the geometric data to high-quality FE models. Section 2 discusses the preprocessing of geometric data, corrections of the geometrical errors, and development of congruent FE meshes for the matrix and reinforcements. The steps for FE model preparation, including assignment of the material properties and application of boundary conditions are described in Section 3. The examples of simulations, performed using the proposed approach, are presented in Section 4.

2. Finite element meshing of a unit cell

Meso-scale FE models of 3D woven composites are usually developed for a *unit cell* (UC) – the smallest repetitive portion of a composite, such that the entire material can be represented as a continuous assemblage of such portions (Fig. 3). Interaction of the UC with surrounding material is modeled by assigning periodic

boundary conditions which require that boundaries of the UC deform in a way that preserves material continuity. Implementation of the periodic boundary conditions is presented in Section 3.

The proposed approach to meshing of 3D woven composites is illustrated by considering the geometry of reinforcement obtained from fabric mechanics simulations in DFMA. DFMA modeling process begins by defining the overall characteristics of a UC, such as the number of warp and weft columns and layers, column spacing, weave pattern, and the cross-sectional area of yarns. Based on this input, the program generates an initial pattern with yarns represented as single cylindrical fibers (Fig. 4). In the next steps of the simulation, each yarn is gradually subdivided into the bundles of sub-yarns subjected to tensile forces. The deformation of woven fabric is modeled by relaxation of these forces. The deformed fabric at the final step of simulations produces the as-woven textile geometry which is required for the development of FE mesh of composites.

2.1. Development of yarn surface mesh

There are two options for output of as-woven yarn geometry in DFMA: stereolithography (STL) format and DFMA geometry (DFMA GEO) format. STL file [12] contains a connectivity table, the corresponding vertex coordinates and normal vectors of triangular surface mesh elements representing the output geometry. DFMA GEO file contains coordinates of points defining the outlines of yarn profiles (“point clouds”). The point clouds are organized in sets of cross-sectional profiles describing each yarn. They can be used in surface reconstruction algorithms [13–16] to generate yarn surfaces. The detailed structure of DFMA GEO file is shown in Fig. 5.

Because of its universality, STL format was initially chosen by the authors. However, in the currently available version of DFMA (0.4.3), STL output can be unstable for large models (the software sometimes crashes during export of models with large numbers of fibers). That is why the point cloud format was selected for generation of the composite reinforcement geometry.

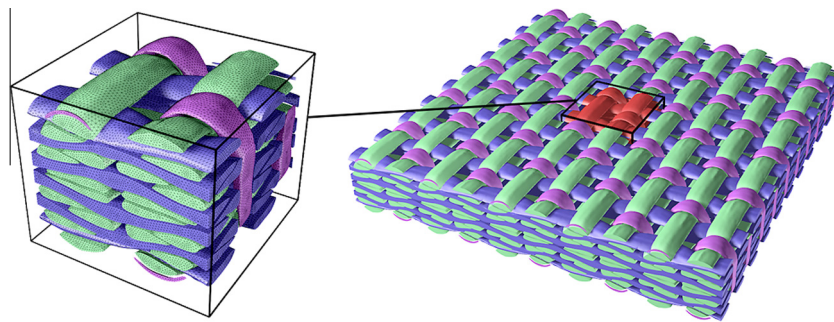


Fig. 3. Unit cell of a 3D woven composite.

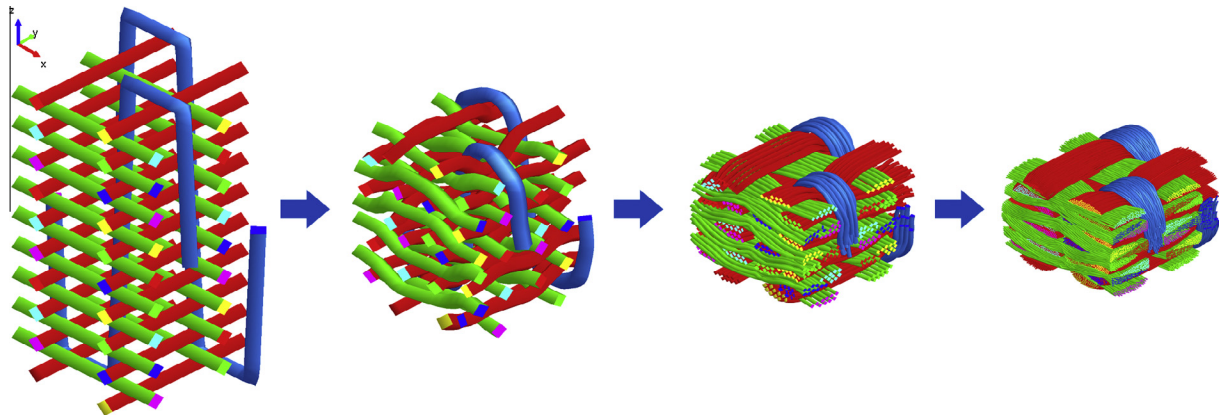


Fig. 4. Modeling steps in DFMA: from initial schematics without sub-yarns to the final as-woven geometry with 80 sub-yarns per yarn.

<BEGINNING OF THE DFMA GEO FILE>		
Number of Yarns: N		
<i>Individual Yarn Information</i>		
<u>Yarn ID</u>	<u>Profiles per Yarn</u>	<u>Points per Profile</u>
I	P_I	Q_I
:	:	:
N	P_N	Q_N
Total Profiles: $P = \sum_{i=1}^N P_i$		
<i>Individual Profile Information</i>		
<u>Profile ID</u>	<u>Yarn ID</u>	<u>Profile Center Coordinates</u>
I	I	$C^I_x \ C^I_y \ C^I_z$
.	.	.
P	N	$C^N_x \ C^N_y \ C^N_z$
$V^I_{IX} \ V^I_{IY} \ V^I_{IZ} \dots$		
$\dots V^I_{Q_I X} \ V^I_{Q_I Y} \ V^I_{Q_I Z}$		
$V^N_{IX} \ V^N_{IY} \ V^N_{IZ} \dots$		
$\dots V^N_{Q_N X} \ V^N_{Q_N Y} \ V^N_{Q_N Z}$		
<END OF THE DFMA GEO FILE>		

Fig. 5. Schematic representation of the DFMA GEO format structure.

One of the problems with generation of UC models from the DFMA output data is that the yarn end caps are not parallel to the UC boundaries, therefore some of the yarns do not reach the boundaries of UC. To deal with the issue, the authors make use of the yarn periodicity conditions implemented in DFMA: the first and the last profiles of yarn's final geometry are of the same shape and orientation. This allows for extension of yarns to the boundaries of UC which is performed during the processing of DFMA GEO output. Processing steps are implemented in a custom MATLAB script that is described in the text to follow.

In the first step of a MATLAB script the yarns are extended in both directions. This is done by duplicating and adding a specified number of profiles to the beginning and end of the yarn. Fig. 6 shows the yarn extension by three profiles in each direction (closed loops represent yarn profiles). The number of extension profiles is chosen such that all end profiles' points lie outside of the unit cell dimensions. Later the excessive yarn elements are cut off to form flat UC surfaces.

The next step in the processing algorithm was specifically developed for better control of the size of FE mesh. At this step, the yarn profiles are re-discretized to a specified number of profile points. This is achieved through interpolation of original profiles by a series of third-degree polynomials with continuous derivatives at the segment endpoints, and subsequent seeding of the interpolated profile. The approach results in smoother refined profile shapes when compared to a simple subdivision of the original profile, see Fig. 7. The level of discretization in the longitudinal yarn direction is controlled by selecting the number of cross-sectional profiles utilized in FE mesh generation.

All yarn profiles are stored in a table as an ordered list of profile points' coordinates. The same order and number of points in profiles within a yarn makes finding coordinates of any point on the yarn surface quite straightforward. This organization scheme is particularly useful when profile "point clouds" are converted to FE meshes. Mesh generation then reduces to assembling a connectivity table. The order in which elements are connected is shown in Fig. 8, where $1, 2, \dots, j, j+1, \dots, Q$ represent local point numbers within the current profile; Q is the number of points in the profile; $k, k+1, l, l+1$ are the point numbers counting from the first point in the current yarn ($k = Q \cdot i + j, l = Q \cdot (i+1) + j'$); $m, (m+1)$ are the element numbers in the connectivity table ($m = 2k - 1$).

For example, the connectivity table entry for element m is $[k, k+1, l]$ and element $m+1$ is $[k+1, l+1, l]$. Once the element con-

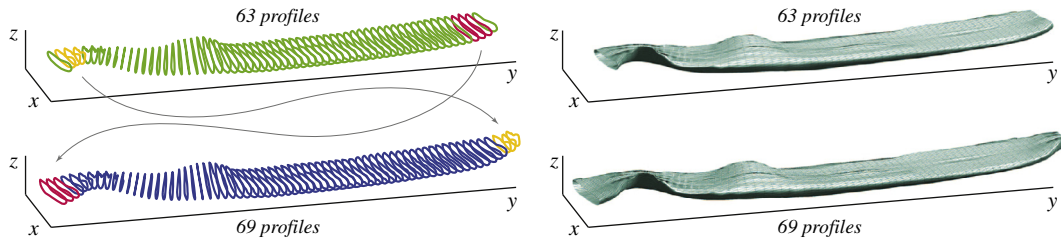


Fig. 6. Illustration of yarn extension procedure based on the duplication and addition of a specified number of profiles to the beginning and end of the yarns.

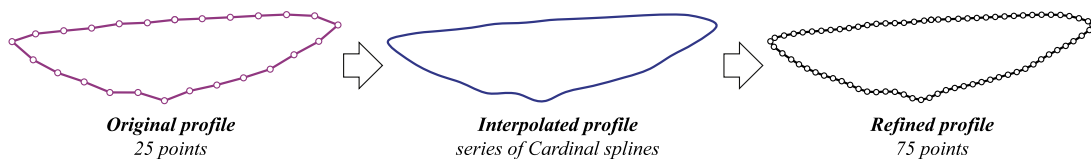


Fig. 7. Profile interpolation and refinement.

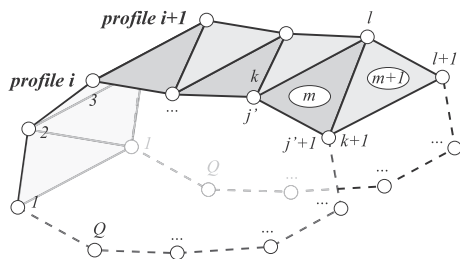


Fig. 8. Schematics of the point order in the element connectivity table.

nectivity table is generated for the entire yarn, Taubin's surface fairing algorithm [17] is applied to the mesh to smooth out the sharp corners of yarns. Note that with the choice of Taubin's parameters $\lambda = 0.5$ and $\mu = -0.5$, as recommended in [18], application of the smoothing algorithm does not result in a yarn's volume change. The yarn element connectivity table is stored along with the updated point coordinates as a MATLAB patch object, and then exported as an STL file using STLWRITE function (see MATLABCentral website).

Before proceeding to the next step of mesh preparation, it is important to check whether periodicity of the yarn geometry is satisfied. In some woven configurations, yarns protrude beyond the dimensions of UC both longitudinally and transversely. Since only one copy of each yarn in the UC is exported from DFMA software, it may be needed to duplicate some yarns to the opposite sides of UC to ensure shape periodicity after the model is cut to the UC dimensions. This step can be performed in any CAD or FEA preprocessing package, e.g. Solidworks or MSC Patran.

2.2. Detection and repair of yarn interpenetrations

One of the major obstacles in numerical analysis of 3D woven composites is that the generated geometric models often contain nonphysical artifacts, which are manifested as portions of two yarns occupying the same volume in space (*yarn interpenetration*). Although this issue is more common when modeling is based on the nominal geometry, it sometimes occurs when the as-woven approach is utilized. Any instance of two surface elements penetrating each other produces an error during meshing with volume elements. Several ways of dealing with this problem have been proposed in the literature including semi-automatic yarn deformation simulations [6], manual manipulations (rotations and shape

changes) of portions of the yarns [5,7], and model-wide reductions of yarn cross-sections [1]. The first method involves subdivision of the UC into portions, each containing only one instance of interpenetration between two yarns, and then shifting and deforming of interpenetrating portions of the yarns. This method works well for geometries with shallow interpenetrations of two adjacent yarns. However, for the cases of deep interpenetration of several adjacent yarns, this method may be difficult to implement due to the limitation of repair of two yarns at a time. This can lead to the lockup of solution because each repair affects another interpenetration instance and does not allow to treat all interpenetrations of a yarn simultaneously. The second method requires extensive manual processing and may result in unrealistic topologies. The third method may lead to a significant loss of reinforcement volume fraction.

The most crucial part in penetration repair is performing the penetration detection in a way that correctly identifies all interpenetrating volumes using the yarn surface data. This step can be implemented as a mesh-based or voxel-based. One example of a mesh-based algorithm is checking whether a potentially penetrating vertex is on the "wrong" side of the host element [19]. Note that we use the term "host" for the yarn whose interior is checked for the presence of penetrating vertices. Another algorithm involves checking whether element edges of the potentially penetrating element intersect the host element [20]. The first approach works reasonably well for shallow penetrations in relatively convex objects. However it results in false positives/negatives (depending on the parameters) for thin or concave objects and deep penetrations. The second method works well for identification of intersecting elements; however, it is not immediately known which vertices are inside of the host body if they do not belong to the intersecting elements (case of deep penetrations).

The major challenge of the surface mesh-based algorithms is that surface meshes do not contain volume information. An entirely different class of penetration detection and repair methods addressing this challenge is based on conversion of meshes to voxel representations, with subsequent Boolean operations on voxels and conversion back to FE meshes [21]. The issue with such approaches is aliasing (jaggedness of boundaries) of meshes generated from voxels, which can be alleviated by applying one of the fairing algorithms, e.g. Taubin's Smoothing [18].

Authors of this paper propose a hybrid approach that combines the two classes of methods described above. To identify penetrations, a voxel representation of the host object is constructed. Voxelization is performed using the parity count algorithm, see [21]. Then all vertices of the remaining objects lying inside of the host

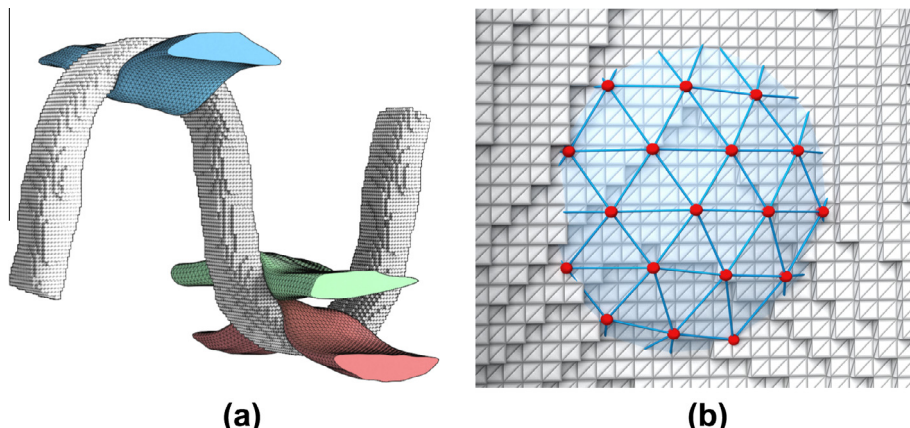


Fig. 9. (a) Voxel representation of the host yarn with three yarns that potentially penetrate the host yarn; (b) illustration of vertex penetration (solid spheres) through voxel representation of the host yarn boundaries.

body voxels are deemed penetrating vertices. Fig. 9a shows a voxel representation of a host yarn with three potentially penetrating yarns. In Fig. 9b, the penetrating vertices inside the host yarn are shown as solid spheres protruding through the voxel representation of yarn boundaries. To repair the penetrations, the penetrating vertices are moved outside of the host yarn in the direction of mean normal of all surface elements inside the host. When there are no vertices left with the coordinates inside the voxels of host body, the penetration is assumed to be repaired. The described algorithm is strongly influenced by the voxel resolution. Too small of a voxel will drastically increase the computational cost, while too large of a voxel will result in the distortion of the shape of penetrating body after the penetration repair. In addition, small features of the host yarn may be lost in the voxel representation due to the lack of resolution. It is important to note that the gap between elements of the host and penetrating bodies is dictated by the voxel size. In some cases these issues can be addressed by using a voxel antialiasing algorithm, e.g. Gaussian Smoothing [22,23].

2.3. Development of 3D solid mesh for yarns and matrix in a unit cell

As discussed in Section 2.1, the yarns are extended to protrude beyond UC dimensions to ensure shape periodicity on the opposite sides. After all interpenetrations are eliminated, the yarns can be cut to the final UC dimensions. For meshes with a small number of elements, this can be achieved using various FE preprocessors. However, for models with a large number of elements (in our case, more than 250,000) the use of general purpose commercial packages becomes inefficient. The authors developed a MATLAB script that goes through every element intersected by the cutting planes (planes parallel to XZ and YZ coordinate planes located at the coordinates corresponding to the dimensions of UC), determines the points of intersection, and creates new elements based on these and old points.

Cutting of triangular elements to UC boundaries produces new elements, some of which are of bad aspect ratios and some even have zero areas. Such elements need to be eliminated before proceeding to meshing with 3D elements. This is achieved by using “MeshOnMesh” function in MSC Patran. This step produces uniform mesh that does not contain skewed elements. At the same time, this function allows for flexible adjustment of mesh discretization which is useful for mesh sensitivity studies. The final step before volumetric meshing involves closing the volume of the yarn surface meshes and generating conforming surface mesh of the matrix. For this step, free edges of the yarn mesh are extracted

and used to create yarn end caps and matrix boundaries. The final surface meshes of yarns and the matrix are shown in Fig. 10. Meshing with tetrahedral linear elements of these surfaces is performed in MSC Patran.

The procedure described in this section was successfully used to generate FE meshes of several different 3D woven architectures, as illustrated in Fig. 11. All of these meshes were processed to develop meso-scale FE models using the procedure discussed in Section 3. The results of FE simulations for one of the models (1x1 orthogonal architecture, Fig. 11a) are presented in Section 4, while the other architectures are considered in [24,25].

3. Numerical model preparation

The meshes developed in Section 2 are used to prepare an FE model of the UC. There are several commercial (such as ANSYS, Abaqus, etc.) and open-source (such as CalculiX, OpenFOAM, etc.) software packages suitable for FE modeling. The authors chose to use a commercial FE software MSC Marc/Mentat. All model preparation steps are performed automatically within the MSC Mentat software using a self-written Python script as described in the subsections to follow.

3.1. Topology features and material properties

The mesh is imported into MSC Mentat, which is the graphical pre- and post-processor for MSC Marc FE solver. During the import stage, the reinforcement and matrix meshes are processed separately to preserve the topological features in the unit cell. Each yarn is imported as a separate set of 3D finite elements, allowing to distinguish them in the model and during the post-processing of results. The matrix mesh is imported as a single element set.

Material properties of the matrix phase are prescribed by selecting the constitutive law of mechanical behavior (e.g. elasto-plastic isotropic) and entering the relevant material coefficients. The choice of material properties for the reinforcement phase depends on its microstructure (see Fig. 1). For example, the effective properties of reinforcement, consisting of the bundles of continuous unidirectional fibers (tows), are transversely isotropic and can be estimated using the appropriate micromechanical models, such as Hashin's and Schapery's formulae [26–28,8]. For the multi-physics simulations, additional information for each of the phases has to be assigned, such as thermal, electrical, or electromagnetic properties.

One of the important steps of model preparation for 3D woven composites with anisotropic reinforcement is the assignment of its

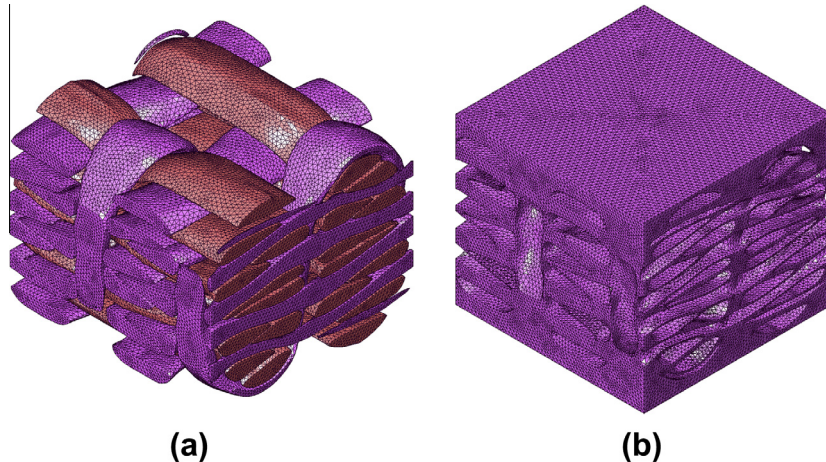


Fig. 10. Final FE surface mesh of the (a) reinforcement and (b) matrix ready for meshing with 3D elements.

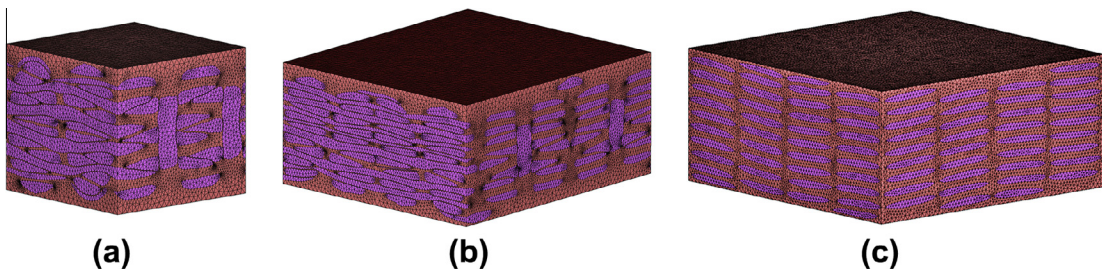


Fig. 11. Examples of the FE meshes generated for: (a) 1 × 1 orthogonal, (b) 2 × 2 orthogonal, and (c) ply-to-ply architectures. Note that the in-plane dimensions of the 1x1 orthogonal UC are two times smaller than that of the other two models.

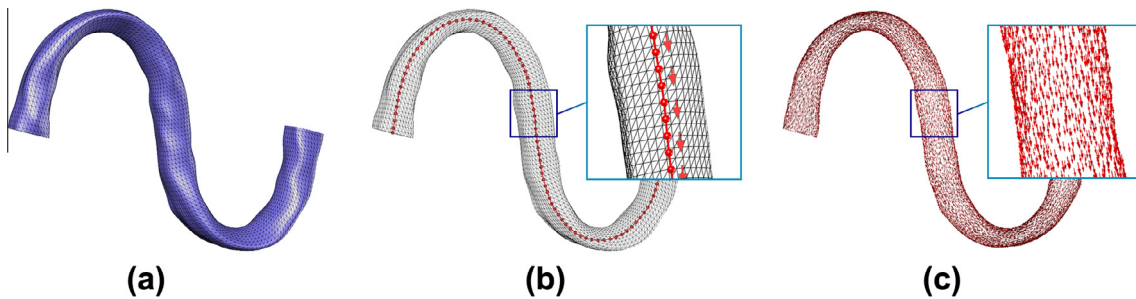


Fig. 12. Assignment of the material orientations for a yarn: (a) FE mesh, (b) center points connected into a polyline, and (c) first principal material orientation based on the mapping of polyline onto FE mesh.

material orientations. Material orientations define the directions of principal material axes in the element relative to the global coordinate system of FE mesh. In our procedure, this information is derived from the point cloud data imported from DFMA (see Section 2.1). In addition to the yarn profile outlines, DFMA output also contains the center points for each of the yarn profiles. These points are consecutively connected into a piecewise linear curve (polyline). The major principal axis for each of the yarn elements is assumed to be coincident with the nearest segment of this polyline (see Fig. 12). The second principal axis is taken in radial direction from the center line to FE centroid. The third principal direction is defined as the vector product of the first two.

3.2. Periodic boundary conditions

In meso-scale FE models, the periodic boundary conditions are prescribed to the boundary surfaces of UC to preserve the material

continuity [29,30]. The UC models of 3D woven composites are usually built for the total thickness of the material, and therefore periodic boundary conditions are imposed on the lateral (warp and weft) directions only. The periodicity condition is necessary to ensure compatibility of the displacement fields on the opposite faces of UC, see for example [31–33]. It is formulated in [31] as:

$$\underline{u}_i^+ = \underline{u}_i^- + \delta_i \quad (i = \text{warp, weft}) \quad (1)$$

where \underline{u}_i^+ and \underline{u}_i^- are the nodal displacements on the positive and negative faces, respectively; δ_i is the average displacement in the i -th direction.

One of the ways to implement the periodic boundary conditions in MSC Marc is to use the option “servo-links” [34]. Servo-links allow to prescribe multi-point boundary conditions for nodal displacements expressed as a linear function with constant coefficients. In this formulation, δ_i is prescribed by creating a

new unconstrained node, and linking the nodes on the corresponding opposite faces on a UC to this node.

However, this implementation of periodic boundary conditions requires a congruent mesh (i.e. same FE configuration and same locations of the FE nodes) of the opposite faces of UC. It is hard to satisfy this condition simultaneously with the requirement for mesh quality during the mesh optimization step discussed in Section 2. To overcome the issue of incongruent mesh, we propose to use the “glue contact” feature of MSC Marc. This feature allows to glue together (i.e. generate automatic nodal ties) of incongruent meshes. In this case, one of the faces of UC is copied as a set of planar elements and glued to the opposite side. Then the periodic boundary conditions are imposed by linking the nodes on one of the faces of UC and its planar copy glued to the opposite face. The glue contact maps the displacements of planar copy to the actual nodes of the opposite face. The proposed approach is illustrated in Fig. 13.

The geometric and material properties of the added planar elements are selected such that their presence has negligible additional effect on the behavior of UC. The negligible effect is defined here as a relative change in the displacement field and effective elastic properties lower than 0.0001%. Based on the sensitivity studies, we propose to assign the thickness of added planar elements to be at most 0.001 of the UC length in the direction normal to the glued face, and stiffness to be at least one order of magnitude lower than that of the most compliant phase of the UC.

3.3. Elimination of rigid body motion

Static FE simulations of the mechanical behavior of UC require to restrain any rigid body motion (both displacements and rotations) without introducing any artificial strains. This can be easily achieved for objects having the shape of right cuboids by fixing, for example, one of the corner nodes in all directions, and restraining two more corners to in-plane motion. However, with the periodic boundary conditions prescribed to all nodes on the boundary surfaces of UC, and without the requirement to keep them flat, this issue requires a special treatment. The approach chosen by the authors is to introduce soft springs, which “suspend” the UC in space, and therefore stabilize the model to allow static solution. This approach is implemented by adding three orthogonal truss elements at each of the corners, as illustrated in Fig. 14. The geometric and material properties of truss elements are selected such that the springs are stiff enough to stabilize the model, but also relatively soft to have negligible effect on the mechanical behavior of UC. Based on the sensitivity studies, we propose the stiffness of

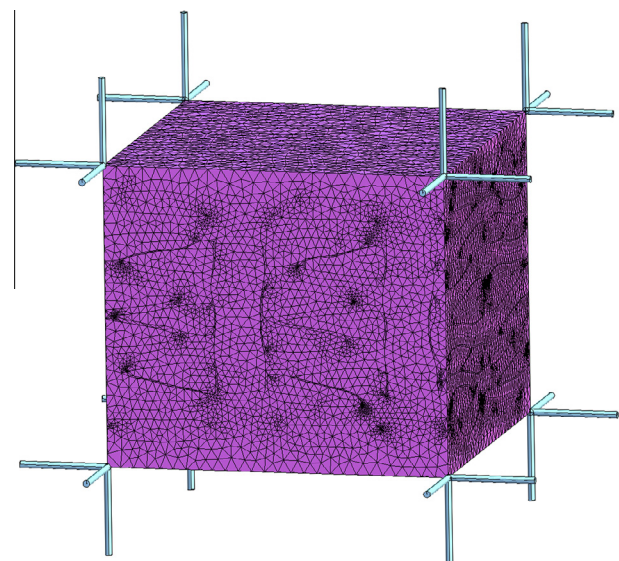


Fig. 14. Soft springs added to restrain the model from rigid body motion.

springs to be about 4–6 orders of magnitude lower than the stiffness of the most compliant phase of the UC.

3.4. Loadcases

The final steps of the model preparation are to define the loadcases, implement the relevant initial and boundary conditions (such as prescribed forces or displacements), and create jobs for MSC Marc solver. The job parameters include selection of the convergence criterion, matrix solver, parallelization options, output quantities, etc. The following parameters were used for the simulations described in Section 4: residuals and displacements convergence criteria with tolerance of 10^{-4} , iterative matrix solver with tolerance of 10^{-8} , four manually prescribed parallelization domains (for discussion of domain decomposition techniques see [35]), binary results file with stress and strain tensors. At the completion of the model preparation Python script, a user is presented with the ready-to-run model. Use of a Python script for automatic model preparation not only streamlines and speeds up the routine process of model preparation, but also ensures uniformity of the simulation results data. This, in turn, simplifies the post-processing

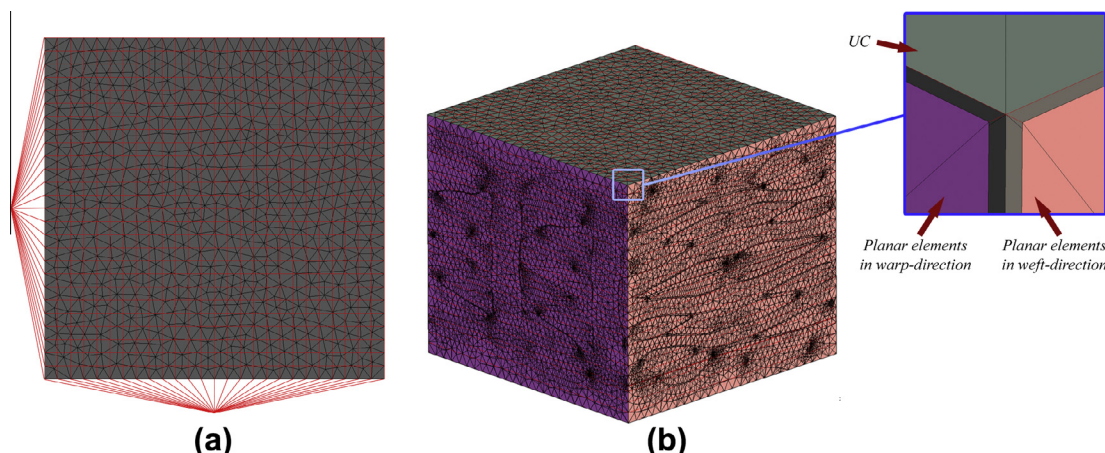


Fig. 13. Implementation of the periodic boundary conditions: (a) top view of UC showing links connecting the opposite faces of UC and the control points; (b) additional planar elements glued to the external faces for mesh congruity.

of large number of simulations of 3D woven composites with different architectures.

4. Examples of numerical simulations

In this section we demonstrate flexibility of the proposed approach for meso-scale FE modeling of 3D woven composites on several cases studies for 1×1 orthogonal reinforcement architecture (see Figs. 1 and 3). We consider four models based on this reinforcement geometry:

1. *Base* model with FE mesh size chosen such that the UC is discretized in approximately 2 million linear tetrahedrons.
2. *Quadratic* model with the same discretization as the *base* model, but linear elements are converted to the second-order isoparametric tetrahedrons.
3. *Refined* model with FE mesh size chosen such that the mesh of linear elements has approximately the same number of nodes as the *quadratic* model.
4. *Reduced* model with reduced volume fraction (VF) of the reinforcement, as compared to the *base* model, and FE discretization similar to that of the *base* model.

The details of FE mesh for each of the models are provided in Table 1. All simulations were performed using MSC Marc/Mentat on a Linux workstation with Intel i7-3770 CPU and 32 GB of RAM. All models were assigned the same set of material properties, and subjected to the same set of loadcases.

4.1. Material properties

The same material properties of the constituents are used in all models. The matrix is assigned the isotropic material properties of RTM6 epoxy resin with Young's modulus $E^{(m)} = 2.9$ GPa and Poisson's ratio $\nu^{(m)} = 0.3$. The reinforcement is assumed to be a transversely isotropic material that represents the resin impregnated 12,000 carbon fibers with 80% volume fraction of fibers within the yarns. The following effective properties of yarns are used [36]: $E_1^{(y)} = 221.4$ GPa, $E_2^{(y)} = 12.6$ GPa, $G_{12}^{(y)} = 7.4$ GPa, $\nu_{12}^{(y)} = 0.34$, $\nu_{23}^{(y)} = 0.32$. Symbols E , G , ν are the Young's modulus, shear modulus, and Poisson's ratio, correspondingly; direction 1 is longitudinal (yarn direction), and directions 2 and 3 are transverse. The material orientations for reinforcement phase are assigned as described in Section 3.1.

4.2. Loadcases

The models described in Table 1 are used to simulate the mechanical behavior of a composite material subjected to 6 loadcases: 3 uniaxial tension and 3 pure shear cases as shown in Table 2. X-axis is chosen in the warp direction, y-axis is in the weft direction, and z-axis is in directed through the thickness. We assume that the overall behavior of the composite is orthotropic as dictated by its microstructure. The components of average strain and stress in this case are related by the effective compliance matrix:

Table 2
Description of the loadcases.

Prescribed strain	Loadcase					
	1	2	3	4	5	6
$\bar{\varepsilon}_{xx}$	0.001	0	0	0	0	0
$\bar{\varepsilon}_{yy}$	0	0.001	0	0	0	0
$\bar{\varepsilon}_{zz}$	0	0	0.001	0	0	0
$\bar{\gamma}_{xy}$	0	0	0	0.001	0	0
$\bar{\gamma}_{yz}$	0	0	0	0	0.001	0
$\bar{\gamma}_{zx}$	0	0	0	0	0	0.001

Table 3
Effective elastic parameters for the considered models. Young's and shear module are given in GPa. The changes in predictions compared to the *base* model are provided in parentheses.

Elastic constant	Model			
	Base	Quadratic	Refined	Reduced
E_x	58.3	56.0	55.7	52.0 (-10.8%)
E_y	54.0	50.8	50.2	47.5 (-12.0%)
E_z	8.42	7.97	8.5	7.74 (-8.1%)
v_{yz}	0.578	0.601	0.569	0.557 (-3.6%)
v_{zx}	0.070	0.072	0.075	0.071 (1.4%)
v_{xy}	0.062	0.060	0.063	0.065 (4.8%)
G_{yz}	1.80	1.57	1.67	1.67 (-7.2%)
G_{zx}	1.95	1.72	1.87	1.83 (-6.2%)
G_{xy}	4.01	3.85	3.79	3.50 (-12.7%)

$$\begin{Bmatrix} \bar{\varepsilon}_{xx} \\ \bar{\varepsilon}_{yy} \\ \bar{\varepsilon}_{zz} \\ \bar{\varepsilon}_{yz} \\ \bar{\varepsilon}_{zx} \\ \bar{\varepsilon}_{xy} \end{Bmatrix} = \begin{bmatrix} 1/E_x & -\nu_{yx}/E_y & -\nu_{zx}/E_z & 0 & 0 & 0 \\ -\nu_{xy}/E_x & 1/E_y & -\nu_{zy}/E_z & 0 & 0 & 0 \\ -\nu_{xz}/E_x & -\nu_{yz}/E_y & 1/E_z & 0 & 0 & 0 \\ 0 & 0 & 0 & 1/G_{yz} & 0 & 0 \\ 0 & 0 & 0 & 0 & 1/G_{zx} & 0 \\ 0 & 0 & 0 & 0 & 0 & 1/G_{xy} \end{bmatrix} \cdot \begin{Bmatrix} \bar{\sigma}_{xx} \\ \bar{\sigma}_{yy} \\ \bar{\sigma}_{zz} \\ \bar{\sigma}_{yz} \\ \bar{\sigma}_{zx} \\ \bar{\sigma}_{xy} \end{Bmatrix}, \quad (2)$$

where $\bar{\sigma}_{ij} = \frac{1}{V} \int_V \sigma_{ij} dV$ are the average stress components; and $\bar{\varepsilon}_{ij} = \frac{1}{V} \int_V \varepsilon_{ij} dV$ are the average strain components in the UC of volume V ; $i, j = x, y, z$.

The effective elastic parameters E_x , E_y , E_z , v_{xy} , v_{yz} , v_{zx} , G_{xy} , G_{yz} , G_{zx} are found using Eq. (2) with the average values of strains and stresses from the corresponding loadcases. Note that substitution of the simulation results from uniaxial tension loadcases can result in slightly different predictions for off-diagonal terms. For example, the value of v_{xy} obtained from loadcase 1 (relation between $\bar{\varepsilon}_{xx}$ and $\bar{\sigma}_{yy}$) can differ from the value obtained from loadcase 2 (relation between $\bar{\varepsilon}_{yy}$ and $\bar{\sigma}_{xx}$). This can be attributed to discretization and round-off error in FE analysis, as well as to the deviations of actual microstructure from the assumed orthotropic symmetry. These differences in predictions of Poisson's ratios for all models are less than 5%.

4.3. Results

Table 3 presents a complete set of the orthotropic elastic properties for 1×1 orthogonal woven composite, calculated with *base*, *quadratic* and *refined* models (columns 2–4 of Table 3). The results for *reduced* model (with the reinforcement volume fraction re-

Table 1

Overall characteristics of FE meshes and volume fractions of reinforcement of the case study models.

Model	Elements (millions)	Nodes (millions)	Mesh type	VF
Base	2.39	0.41	4-Node linear tetrahedron	0.66
Quadratic	2.39	3.23	10-Node quadratic tetrahedron	0.66
Refined	19.1	3.23	4-Node linear tetrahedron	0.66
Reduced	2.31	0.39	4-Node linear tetrahedron	0.58

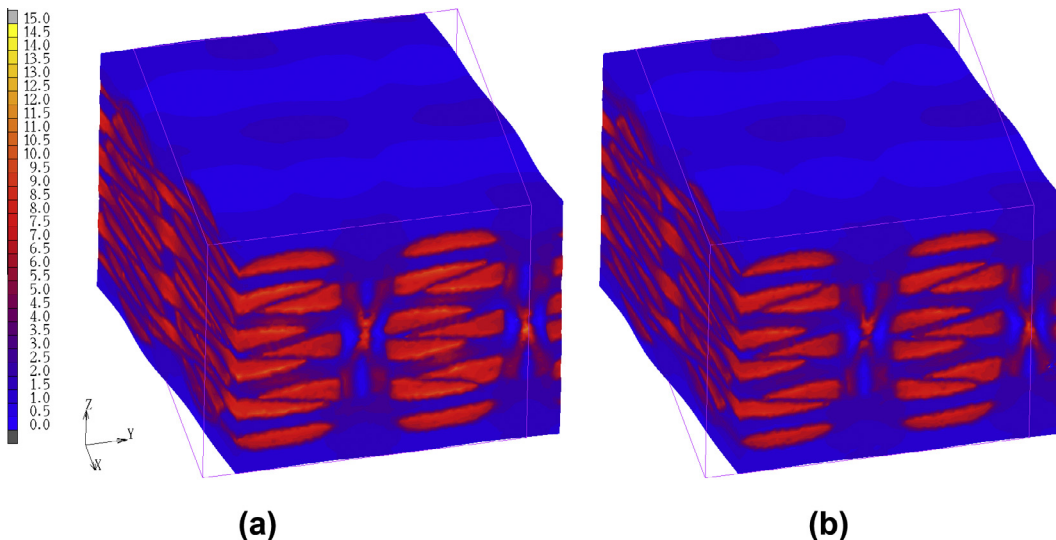


Fig. 15. Distribution of xy stresses in the (a) *base* and (b) *reduced* models subjected to loadcase 4 (pure shear in xy direction). Deformations are exaggerated by a factor of 200.

duced by 12% from 0.66 to 0.58) are also provided for comparison. It can be seen that the predictions obtained with the initial level of discretization, *base* model, can be improved by either using quadratic elements with more integration points per element or refining the FE mesh. For example, the *base* model overpredicts the in-plane stiffness (characterized by E_x , E_y , G_{xy}) on average by 4.85%. Note that the improvement due to the use of quadratic elements (more degrees of freedom for the same mesh) is somewhat limited because the material orientations are defined on per-element basis. Thus, for complex topologies, a refined mesh is needed for accurate representation of material orientations for composites with anisotropic constituents.

Analysis of the obtained effective elastic properties for the model with *reduced* amount of reinforcement shows that the predicted reduction in the stiffness is approximately proportional to the reduction in the volume fraction of reinforcement (see columns 2 and 5 of Table 3). This effect is more pronounced for the in-plane stiffness parameters (E_x , E_y , G_{xy}). Note that the distribution of stresses for *base* and *reduced* models exhibits a similar pattern, as illustrated by the contour plot of shear stresses, σ_{xy} , for loadcase 4 (see Fig. 15).

5. Conclusions

The procedure developed in this paper provides an automated tool to generate FE models of 3D woven composites based on the topology data in point cloud or STL format, as available from DFMA simulations. The yarn interpenetration issue, very common in woven composite material modeling, is resolved by an algorithm which does not significantly reduce the volume fraction of reinforcement. Periodic boundary conditions are assigned to the lateral surfaces obtained by processing of the reinforcement topology data. The material orientations in finite elements of the yarns are assigned based on the direction of central line at the point closest to the FE centroid.

The proposed procedure can be readily implemented in a scripting language compatible with a FE software package of choice. The authors used MATLAB and Python scripts with MSC Marc/Mentat FE software. The demonstrated examples show that the meso-scale models with 1–10 million degrees of freedom can be developed and run on the presently available consumer-grade workstation (single CPU with 32 GB of RAM) in reasonable time. For example,

preprocessing of the *base* model takes about 2 h, and FE simulations take about 10 min of CPU time.

Acknowledgements

This material is based upon work supported by the National Science Foundation under Grant No. CMMI-1100409. This research was performed in collaboration with Albany Engineered Composites (AEC), Inc., and also supported by the New Hampshire Innovation Research Center. The authors thank Michael Giovinazzo (AEC) for providing the geometric data. We are also grateful to Harun Bayraktar, Jon Goering (AEC) and Todd Gross (UNH) for helpful discussion of the mechanics of 3D woven composites.

References

- [1] Lin Hua, Brown Louise P, Long Andrew C. Modelling and simulating textile structures using TexGen. *Adv Mater Res* 2011;331(September):44–7.
- [2] Verpoest Ignas, Lomov Stepan V. Virtual textile composites software WiseTex: integration with micro-mechanical, permeability and structural analysis. *Compos Sci Technol* 2005;65(15–16):2563–74.
- [3] Tong Liyong, Mouritz Adrian P, Bannister Michael K. 3D Fibre reinforced polymer composites, Kidlington, UK; 2002.
- [4] Bogdanovich Alexander E. Multi-scale modeling, stress and failure analyses of 3-D woven composites. *J Mater Sci* 2006;41(20):6547–90.
- [5] Sherburn Martin. Geometric and mechanical modelling of textiles. Phd dissertation, University of Nottingham; 2007.
- [6] Lomov Stepan V, Ivanov Dmitry S, Verpoest Ignas, Zako Masaru, Kurashiki Tetsusei, Nakai Hiroaki, et al. Meso-FE modelling of textile composites: road map, data flow and algorithms. *Compos Sci Technol* 2007;67(9):1870–91.
- [7] Rinaldi Renaud G, Blacklock Matthew, Bale Hrishikesh, Begley Matthew R, Cox Brian N. Generating virtual textile composite specimens using statistical data from micro-computed tomography: 3D tow representations. *J Mech Phys Solids* 2012;60(8):1561–81.
- [8] Tsukrov Igor, Bayraktar Harun, Giovinazzo Michael, Goering Jon, Gross Todd, Fruscello Monica, et al. Finite element modeling to predict cure-induced microcracking in three-dimensional woven composites. *Int J Fract* 2011;172(2):209–16.
- [9] Wang Youqi, Sun Xuekun. Digital-element simulation of textile processes. *Composites Science and Technology* 2001;61(2):311–9.
- [10] Zhou Guangming, Sun Xuekun, Wang Youqi. Multi-chain digital element analysis in textile mechanics. *Compos Sci Technol* 2004;64(2):239–44.
- [11] Miao Yuyang, Zhou Eric, Wang Youqi, Cheeseman Bryan A. Mechanics of textile composites: micro-geometry. *Compos Sci Technol* 2008;68(7–8):1671–8.
- [12] Rypl Daniel, Bittnar Zdeněk. Triangulation of 3D surfaces recovered from STL grids. *Acta Polytech* 2004;44(5–6):61–7.
- [13] Rypl Daniel, Bittnar Zdeněk. Direct triangulation of 3D surfaces using the advancing front technique. In: Proceedings of the second ECCOMAS conference on numerical methods in engineering; 1996.

- [14] Bernardini Fausto, Mittleman Joshua, Rushmeier Holly, Silva Claudio, Taubin Gabriel. The ball-pivoting algorithm for surface reconstruction. *IEEE Trans Visual Comput Graph* 1999;5(4):349–59.
- [15] Rypl Daniel, Bittnar Zdeněk. Triangulation of 3D surfaces reconstructed by interpolating subdivision. *Comput Struct* 2004;82(23–26):2093–103.
- [16] Kazhdan Michael, Bolitho Matthew, Hoppe Hugues. Poisson surface reconstruction. In: Eurographics symposium on geometry processing; 2006. p. 61–70.
- [17] Taubin Gabriel. Curve and surface smoothing without shrinkage. In: Proceeding of the fifth international conference on computer vision; 1995. p. 852–857.
- [18] Taubin Gabriel. A signal processing approach to fair surface design. In: Proceedings of SIGGRAPH 95; 1995. p. 351–358.
- [19] Li Jituo, Ye Juntao, Wang Yangsheng, Bai Li, Lu Guodong. Fitting 3D garment models onto individual human models. *Comput Graph* 2010;34(6):742–55.
- [20] Möller Tomas, Trumbore Ben. Fast, minimum storage ray-triangle intersection. *J Graph Tools* 1997;2(1):21–8.
- [21] Nooruddin Fakir S, Turk Greg. Simplification and repair of polygonal models using volumetric techniques. *IEEE Trans Visual Comput Graph* 2003;9(2):191–205.
- [22] Lindeberg Tony. Scale-space for discrete signals. *IEEE Trans Pattern Anal Mach Intel* 1990;12(3):234–54.
- [23] Bülow Thomas. Spherical diffusion for 3D surface smoothing. *IEEE Trans Pattern Anal Mach Intel* 2004;26(12):1650–4.
- [24] Drach Andrew, Drach Borys, Tsukrov Igor, Bayraktar Harun, Goering Jon. Realistic FEA modeling of 3D woven composites on meso-scale. In: 19th International conference on composite materials (ICCM19), Montreal, Canada; 2013.
- [25] Tsukrov Igor, Drach Borys, Bayraktar Harun, Goering Jon. Modeling of cure-induced residual stresses in 3D woven composites of different reinforcement architectures. *J Key Eng Mater*, in press.
- [26] Hashin Zvi, Walter Rosen B. The elastic moduli of fiber-reinforced materials. *J Appl Mech* 1964;31(2):223.
- [27] Hashin Zvi. Analysis of properties of fiber composites with anisotropic constituents. *J Appl Mech* 1979;46(3):543.
- [28] Schapery RA. Thermal expansion coefficients of composite materials based on energy principles. *J Compos Mater* 1968;2(3):380–404.
- [29] van der Sluis O, Schreurs PJG, Brekelmans WAM, Meijer HEH. Overall behaviour of heterogeneous elastoviscoplastic materials: effect of microstructural modelling. *Mech Mater* 2000;32(8):449–62.
- [30] Li Shuguang. General unit cells for micromechanical analyses of unidirectional composites. *Compos A: Appl Sci Manuf* 2001;32(6):815–26.
- [31] Xia Zihui, Zhang Yunfa, Ellyin Fernand. A unified periodical boundary conditions for representative volume elements of composites and applications. *Int J Solids Struct* 2003;40(8):1907–21.
- [32] Xia Zihui, Zhou Chuwei, Yong Qiaoling, Wang Xinwei. On selection of repeated unit cell model and application of unified periodic boundary conditions in micro-mechanical analysis of composites. *Int J Solids Struct* 2006;43(2):266–78.
- [33] Kopernik Magdalena, Milenin Andrzej. Two-scale finite element model of multilayer blood chamber of POLVAD_EXT. *Arch Civil Mech Eng* 2012;12(2):178–85.
- [34] MSC Software. MSC Marc 2012 User Documentation. Volume A: theory and user information. Technical report, MSC Software, Santa Ana, CA, USA; 2012.
- [35] Krysl Petr, Bittnar Zdeněk. Parallel explicit finite element solid dynamics with domain decomposition and message passing: dual partitioning scalability. *Comput Struct* 2001;79:345–60.
- [36] Tsukrov Igor, Giovinazzo Michael, Vyshenska Kateryna, Bayraktar Harun, Goering Jon, Gross Todd. Comparison of two approaches to model cure-induced microcracking in three-dimensional woven composites. In: Proceedings of the ASME 2012 international mechanical engineering congress and exposition, Houston, TX; 2012.